Modification Mechanism of Polyamide Reverse Osmosis Membrane by Persulfate: Roles of Hydroxyl and Sulfate Radicals

Wei Cheng, Haodan Xu, P Wang, Lihong Wang, Anthony Szymczyk, Jean-Philippe Croué, Tao Zhang

Modification Mechanism of Polyamide Reverse Osmosis Membrane by Persulfate: Roles of Hydroxyl and Sulfate Radicals

Submitted to

Environmental Science & Technology

April 19, 2022

Authors

Wei Cheng,[1] Haodan Xu,[1] Peizhi Wang,[1,2] Lihong Wang,[1] Anthony Szymczyk,[3] Jean-Philippe Croué,[4] Tao Zhang[1,*]

[1] Research Center for Eco-Environmental Sciences, Chinese Academy of Sciences, Beijing 100085, China
[2] School of Civil and Environmental Engineering, Shenzhen Key Laboratory of Water Resource Application and Environmental Pollution Control, Harbin Institute of Technology (Shenzhen), Shenzhen 518055, China
[3] Université de Rennes, CNRS, ISCR – UMR 6226, F-35000, Rennes, France
[4] Institut de Chimie des Milieux et des Matériaux IC2MP UMR 7285 CNRS, Université de Poitiers, France

*corresponding author
Email: taozhang@rcees.ac.cn (T. Zhang)
Tel: 86 10 62849628

TOC Art

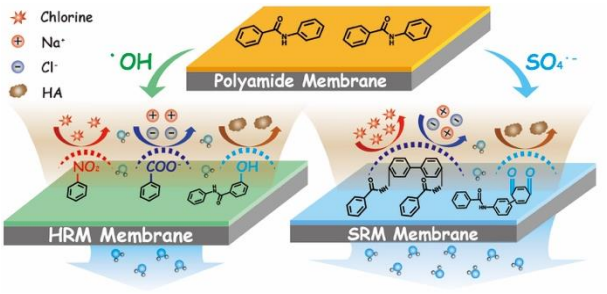
Chlorine
Na+
Cl-
HA
·OH
Polyamide Membrane
SO4·-
NO2
COO-
OH
HRM Membrane
SRM Membrane

ABSTRACT

Oxidative modification is a facile method to improve the desalination performance of thin-film composite membranes. In this study, we comparatively investigated the modification mechanisms induced by sulfate radical ($SO_4^{\bullet-}$) and hydroxyl radical ($HO^{\bullet}$) for polyamide reverse osmosis (RO) membrane. The $SO_4^{\bullet-}$- and $HO^{\bullet}$-based membrane modifications were manipulated by simply adjusting the pH of the thermal-activated persulfate solution. Although both of them improved water permeability of the RO membrane under certain conditions, the $SO_4^{\bullet-}$-modified membrane notably prevailed over the $HO^{\bullet}$-modified one due to higher permeability, more consistent salt rejection rates over wide pH and salinity ranges, and better stability when exposed to high doses of chlorine. The differences of the membranes modified by the two radical species probably can be related to their distinct surface properties in terms of morphology, hydrophilicity, surface charge, and chemical composition. Further identification of the transformation products of a model polyamide monomer using high-resolution mass spectrometry demonstrated that $SO_4^{\bullet-}$ initiated polymerization reactions and produced hydroquinone/benzoquinone and poly-aromatic structures; whereas the amide group of the monomer was degraded by $HO^{\bullet}$, generating hydroxyl, carboxyl, and nitro groups. The results will enlighten effective ways for practical modification of polyamide RO membranes to improve desalination performances and the development of sustainable oxidation-combined membrane processes.

KEYWORDS： *polyamide RO membrane, oxidative modification, hydroxyl radical, sulfate radical, desalination, chlorine resistance, fouling resistance*

SYNOPSIS： Sulfate and hydroxyl radical modification of polyamide RO membrane follow distinct reaction pathways and achieve different desalination performance.

INTRODUCTION

Membrane technology plays an increasingly important role in desalination and water reuse to alleviate the stress of global water scarcity. Currently, reverse osmosis (RO) is leading the membrane application to augment water supply owing to its remarkable efficiency in water-solute separation and energy consumption.[1, 2] Across the substantial investigations on membrane materials, thin film composite (TFC) polyamide membrane, which is characterized by high water permeability, salt rejection, and chemical stability, became a gold standard for RO processes.[3, 4] In recent years, there are increasing demands for developing novel membranes with higher water permeability, which require less energy consumption and fewer membrane elements to be installed for brackish water desalination and wastewater reclamation.[5] However, inherent material limitations of the TFC membrane, such as permeability-selectivity trade-off, seriously hinder the comprehensive improvement of membrane properties.[6, 7] Besides, high water permeance usually aggravates membrane fouling because of the increased concentration polarization phenomenon.

Numerous efforts have been made to improve water permeability and fouling resistance while maintaining high solute rejection for TFC membranes. For example, incorporating nanomaterials into the membrane generates nanochannels inside the polyamide layer for fast water transport;[8, 9] coating/grafting hydrophilic polymers on the membrane surface produces hydrophilic hydrated shells and thus improves membrane flux and mitigates membrane fouling.[10, 11] However, the performance of the functionalized membranes may deteriorate due to potential release of the functional material.[12, 13] Post-treatment of TFC membranes with heating, alkali, or hypochlorite can significantly enhance the membrane permeance by modifying the physicochemical properties of the active layer (e.g., cross-linking degree, hydrophilicity, or thickness).[14-18] These simple treatments are the prevailing surface modification methods in manufacturing, although the operational conditions should be carefully

controlled to avoid destroying the membrane permselectivity.

Recently, oxidative modification with UV and persulfate has been successfully applied to improve the permeability, fouling- and chlorine-resistance of the TFC membrane.[12, 19] UV irradiation of the TFC membrane was delicately conducted in water.[12] The irradiation process breaks the cross-linked bond of polyamide to produce carboxyl and amine groups on the membrane surface, which subsequently increases membrane surface charge and hydrophilicity. Free radicals/reactive oxygen species (ROS) could be generated in the bulk solution or on the membrane surface during UV irradiation.[20, 21] Therefore, there are uncertainties about their functions on membrane properties. Bing et al. used heated persulfate solution at pH 8 to modify the polyamide membrane.[19] They proposed that hydroxyl radical ($HO^{\bullet}$) can modify the TFC membrane via surficial oxidation and interfacial crosslinking, which improves membrane permeability and chlorine resistance. Nevertheless, the speciation of radicals in the persulfate solution is pH dependent. It is well known that sulfate radical ($SO_4^{\bullet-}$) is generated through persulfate decomposition and can convert to $HO^{\bullet}$ in reaction with OH^-.[22, 23] $SO_4^{\bullet-}$ and $HO^{\bullet}$ coexist at near-neutral pH.[22, 23] It is known that the two radical species have distinct reaction pathways towards some organic compounds.[22, 24] Their reactions with surface moieties of the polyamide membrane could be also different. Understanding the fundamental roles played by specific oxidative species will elucidate the intrinsic correlation of membrane performance and material properties and facilitate the development of high-performance TFC membranes.[4]

$HO^{\bullet}$ and $SO_4^{\bullet-}$ are the most referred strong oxidants with reducing potentials of 1.90–2.70 and 2.5–3.1 V, respectively.[24] Generally, $HO^{\bullet}$ prefers to undergo hydrogen abstraction or radical addition with a broad range of organics, while $SO_4^{\bullet-}$ is more prone to electron transfer reactions with higher selectivity towards specific functional groups.[22, 24] We hypothesize that $HO^{\bullet}$ and $SO_4^{\bullet-}$ could react differently with polyamide polymer, considering that the polymer has both unsaturated aromatic moieties and reactive amide groups. Besides, oxidation processes such as H_2O_2, UV/H_2O_2, and

persulfate have been investigated recently in conjunction with membrane filtration processes to mitigate membrane fouling or remove contaminants.[25-27] Catalytic-functionalized TFC membranes were also prepared to alleviate biofouling by in-situ generation of $HO^{\bullet}$.[28, 29] The emergence of these oxidation-combined membrane processes addresses the need for a better understanding of the reactions between oxidative species and polyamide membranes.[30, 31]

This study aims to compare the effectiveness of $HO^{\bullet}$ and $SO_4^{\bullet-}$ for polyamide RO membrane modification and relate the differences to their reaction pathways. By simply adjusting the pH of persulfate solution in thermal activation, the predominance of $HO^{\bullet}$- or $SO_4^{\bullet-}$-modification was manipulated. The effects of modification by the two radicals were comprehensively compared in aspects of water permeability, chlorine- and fouling-resistance as well as solute rejection. To understand the membrane modification mechanism of the two radical species, their reactions with benzanilide (BA), a model polyamide monomer, were also investigated. The reaction pathways were proposed based on transformation product analysis using a quadrupole time-of-flight (QTof) mass spectrometer.

MATERIALS AND METHODS

Membrane and Chemicals. Commercial polyamide RO membranes (SW30XLE and BW30) were purchased from Dow Filmtec^{TM}. Sodium peroxodisulfate (PDS, Sigma-Aldrich) was used as a precursor to generate radical species in solution for membrane modification. Solution pH was adjusted with dilute H_2SO_4 or NaOH. NaCl was purchased from Aladdin (Shanghai, China). Sodium hypochlorite was supplied by Shanghai Hushi Reagent. Benzanilide (BA) and humic acid (HA) obtained from Sigma-Aldrich were used as polyamide monomer and model foulant, respectively.

Oxidation Modification. Thermal activation of PDS at pH 4 and pH 10 was used to induce $SO_4^{\bullet-}$ or $HO^{\bullet}$ generation because of the following considerations. First, PDS can be activated by heat

according to eq (1). $SO_4^{\bullet-}$ generated can convert to $HO^{\bullet}$ under base condition through eq (2). It was also reported that $SO_4^{\bullet-}$ directly reacts with water to produce $HO^{\bullet}$ (eq (3)). However, the reaction rate of eq (3) is very low, meaning that $SO_4^{\bullet-}$ dominates at pH $\leq$ 7.[22]

$$S_2O_8^{2-} + \text{heat} \rightarrow 2SO_4^{\bullet-} \quad (1)$$

$$SO_4^{\bullet-} + HO^- \rightarrow SO_4^{2-} + HO^{\bullet} \qquad k_1 = 6.5 \times 10^7\ M^{-1}\ s^{-1} \quad (2)$$

$$SO_4^{\bullet-} + H_2O \rightarrow SO_4^{2-} + HO^{\bullet} + H^+ \qquad k_2[H_2O] < 2 \times 10^{-3}\ s^{-1} \quad (3)$$

Also, the predominance of $SO_4^{\bullet-}$ at pH 4 and the generation of $HO^{\bullet}$ at pH 10 were further confirmed with a probe compound (i.e., 2,4-dichlorophenol) (Figure S1, SI). Second, the decomposition rate of PDS is independent of its initial concentration and remains to be constant at pH 4 and pH 10 (Figure S2a, SI).[32] During the membrane modification in this study (i.e., 5 h), the PDS decomposed by ~5%, which means that the PDS concentration is relatively constant. In comparison, peroxymonosulfate (PMS)/Co^{2+}, another typical process of $SO_4^{\bullet-}$ generation, induces rapid PMS decomposition (Figure S2b, SI). The persistence of PDS during thermal activation guarantees interaction of the membrane with oxidant species at relatively constant concentrations. Third, the thermal activation of PDS can avoid the impacts of metals and UV irradiation on membrane modification. The influencing factors (i.e., PDS, pH, and heating) on membrane water flux and salt rejection were also tested individually, and negligible impacts of them on membrane performance were observed (Figure S3, SI).

Before modification, the membrane was immersed in isopropanol solution (25 %) for 30 min and washed thoroughly using pure water. Hydroxyl radical modified (HRM) and sulfate radical modified (SRM) membranes were fabricated by immersing the pristine RO membrane in PDS solution for 5 h at 50 °C under base (pH 10) or acidic (pH 4) conditions, which enables controlled $HO^{\bullet}$ or $SO_4^{\bullet-}$ generation. It should be noted that $SO_4^{\bullet-}$ may not completely transfer to $HO^{\bullet}$ at pH 10, although the membrane property variation is mainly caused by the $HO^{\bullet}$ oxidation, which will be discussed in this study. Borate buffer (5 mM) was applied for pH 10. No buffer was used for pH 4 because the solution

147 pH nearly did not change during the membrane modification. After modification, the HRM and SRM
148 membranes were thoroughly rinsed with pure water and stored at 4 °C before use. The concentration
149 of PDS in the solution was measured with a potassium iodide colorimetric method.[33]

150 **Membrane Performance Test.** Water flux and salt rejection of the pristine and modified
151 RO membranes were measured with a bench-scale crossflow filtration system. The surface area of the
152 membrane was 14.6 cm^2. The crossflow velocity was 71.8 cm/s and the water temperature was
153 maintained at 25 ± 0.5 °C. The water flux of RO was measured at 14 bar. Solute rejection was tested
154 with synthetic water containing 10 mM NaCl. Humic acid was used as the model foulant to evaluate
155 the fouling propensity of membranes at pH 7.5 before and after oxidative modification. Detailed
156 information on the membrane performance test and fouling experiment was described in Text S1, SI.

157 **Membrane Characterization.** Surface morphology and roughness of the pristine and
158 modified membranes were characterized by cold field emission scanning electron microscopy (FE-
159 SEM, Hitachi SU8010) and atomic force microscopy (AFM, Bruker FastScan Bio). Surface chemical
160 information of the membranes was analyzed with an infrared spectrometer equipped with an attenuated
161 total reflection accessory (ATR-FTIR, Nicolet iN10MX) and an X-ray photoelectron spectrometer
162 (XPS, Escalab 250Xi). Membrane surface charge at different pH (measuring solution: 1 mM KCl) was
163 measured with a streaming current analyzer (Anton Paar, SurPASS 3). Contact angle of the membrane
164 was determined using an optical goniometer (Data Physics Instruments, OCA20). Surface density of
165 carboxyl groups on the membrane surface was quantified with a silver binding method as described in
166 previous studies.[34, 35] The effective pore size of the membrane was estimated according to a pore
167 transport model utilizing the rejection of reference organic tracers.[36] More details of carboxyl group
168 areal density and pore size measurements are provided in Text S2 and S3, SI.

169 **Reaction of Benzanilide Monomer and Analytical Methods.** The reaction
170 mechanism of the polyamide membrane with oxidative species in PDS solution at different pH was

investigated by using BA as a model polyamide monomer. The BA monomer was dissolved in acetonitrile with a concentration of 50 mM and stored at -20 °C. Various concentrations of PDS (600, 1000, and 2000 μM) were used to react with BA (200 μM) at molar ratios of 3:1, 5:1, and 10:1, respectively, at 50 °C. The pH of the PDS solution was maintained at 10 or ~4 with or without borate buffer. Samples were withdrawn at different time intervals and quenched by quick cooling down to room temperature. The concentration of BA was determined with an HPLC (Waters 2487) equipped with a Phenomenex Luna C18 column (4.6 mm × 150 mm × 5 μm) using isocratic ultrapure water and methanol (50%:50%, v/v) of 1 mL min^{-1} as mobile phase and detection wavelength of 260 nm. BA transformation products were analyzed using a QTof mass spectrometer (X500R, AB SCIEX) operated in the negative (for samples reacted at pH 10) or positive (for samples reacted at pH 4) IDA mode. Accurate mass and empirical formulas of the degradation products were provided by the QTof. Detailed LC and MS settings are described in Text S4, SI. The products were also derivatized with methanol at acid pH for GC/MS analysis. The derivatization method and the GC/MS operating condition are shown in Text S5, SI.

RESULTS AND DISCUSSION

Water Permeability and Salt Rejection of Modified Polyamide Membranes. Water flux and salt rejection of the polyamide membrane before and after oxidative modification were measured with a crossflow RO system. The water fluxes of SRM and HRM membranes were normalized to that of the pristine membrane to clearly present the effect of oxidative modification on the membrane permeability. Oxidative modification of the SW30 membrane under acidic or base conditions significantly improved its water permeability, with higher fluxes being observed under larger PDS doses (Figure 1). For example, the water permeability of SRM^{SW30} and HRM^{SW30} membranes were ~270% and ~190% higher than the pristine SW30 membrane, respectively, after modification at the

PDS dose of 35 g/L. In contrast to the water permeance, radical exposures have a minimal influence on NaCl rejection until the PDS doses increased to 50 g/L. Under this condition, the NaCl rejection decreased to 85.0% and 90.9% for the SRM and HRM membranes, respectively. The results suggest that the oxidative modification at moderate PDS doses can effectively improve the water permeance of the polyamide membrane while maintaining high salt rejection.

Interestingly, the modification at pH 4 (SRM^{SW30}) achieved higher efficiency (i.e., a lower PDS dose is needed to achieve equal improvement of water permeability) than that at pH 10 (HRM^{SW30}). The water permeability increment of the polyamide membrane exerted by PDS modification showed an obvious threshold of PDS dose (i.e., ~10 g/L) at pH 10. In contrast, the water permeability was more sensitive to the PDS dose when the membrane was modified at pH 4. In other words, the polyamide membrane exhibits different reactivity towards the oxidant species generated at pH 4 and 10. Also, the surface color of the SRM^{SW30} membrane was quite different from the HRM^{SW30} (Figure S4, SI). These results imply that the modification mechanism at the two pH values might be different, and may influence the membrane performance in different ways which is the focus of this study.

Figure 1

Surface Characterization of the Modified Membranes. The surface morphology of the pristine and modified SW30 membranes was visualized by SEM and AFM. The oxidative modification was conducted with 4 g/L PDS at pH 4 or 30 g/L PDS at pH 10 to obtain the SRM^{SW30} and HRM^{SW30} membranes, respectively, having comparable water flux and salt rejection. The SRM^{SW30} membrane showed a similar ridge-and-valley structure to the pristine membrane, while this structure slightly dimed and the thickness of the active layer decreased for the HRM^{SW30} membrane (Figures 2a–c and S5) implying degradation of the polyamide layer. This result is consistent with the lower roughness of the HRM^{SW30} membrane (Rq = 68.45 nm) than the SRM^{SW30} (Rq = 76.80 nm). The morphological difference between the HRM^{SW30} and SRM^{SW30} membranes seems contradictory to the

218 difference in their water permeability (Figure 1). We suppose that the change in the material
219 physicochemical properties may play an important role in the filtration performance of the modified
220 membranes.

221 **Figure 2**

222 ATR-FTIR spectra of the pristine and modified SW30 membranes are presented in Figure S6 (SI).
223 Both polyamide and polysulfone layers showed characteristic peaks in the 1000–1800 cm^{-1} range
224 (Figure S6a, SI).[37] Typical peaks that can be assigned to polysulfone include: i) 1584, 1504, and 1487
225 cm^{-1} (aromatic ring), ii) 1411, 1387, 1363 cm^{-1} (C-H moiety), iii) 1322, 1294, 1169, 1148 cm^{-1} (SO_2
226 moiety), and iv) 1239 cm^{-1} (C-O-C moiety).[38] The IR bands of polysulfone before and after
227 modification are quite similar, which implies that the oxidative modification employed in this study
228 has minimal impact on the polysulfone supporting layer. The spectrum recorded for the aromatic
229 polyamide layer presented 3 typical amide bands, i.e., the amide I at 1669 cm^{-1} (C=O stretching), the
230 aromatic amide at 1609 cm^{-1} (N-H or C=C ring vibration), and the amide II at 1541 cm^{-1} (N-H in-
231 plane bending and N-C stretching vibration). The spectrum of the HRM^{SW30} membrane exhibited
232 slightly lower intensity for all the 3 amide peaks, while only aromatic amide and amide II bands
233 attenuated slightly for the SRM^{SW30} membrane. In addition, the characteristic peak of hydroxyl moiety
234 of the residual carboxyl groups at 3380 cm^{-1} [39, 40] became broader for the HRM^{SW30} membrane (Figure
235 S6b, SI), implying that the decomposition of amide may produce extra carboxyl groups.

236 XPS high-resolution scans of C 1s, O 1s, and N 1s can provide additional information on the
237 polyamide layer of the pristine and modified SW30 membranes (Figures 2d, 2e, and S7). Negligible
238 changes of C-C (248.8 eV), C-N or C-OH (286.1 eV), and C=O vibration of amide (288.1 eV) were
239 observed for the SRM^{SW30} membrane.[12, 41] However, a peak assignable to the $\pi \rightarrow \pi^*$ shake-up
240 satellite emerged at 291.4 eV (the inset in Figure 2d). It is likely due to the formation of polycyclic
241 aromatic structures such as biphenyl or multi-phenyls,[42, 43] indicating that $SO_4^{\bullet-}$ generated from PDS

decomposition at the acidic pH may induce polymerization of aromatic rings on the polyamide surface. In contrast, the C-O peak at 286.1 eV shifted to lower binding energy (δ_{BE} = 0.25 eV) with higher intensity for the HRM^{SW30} membrane. The O 1s spectrum of the HRM^{SW30} membrane also showed higher intensity of C-O at 532.7 eV as compared with the pristine membrane (Figure 2e). These results further confirm the oxidative decomposition of the polyamide layer in the basic PDS solution. The N 1s spectrum of the pristine SW30 membrane before and after modification did not show any significant difference (Figure S7, SI).

Surface elemental composition of the membranes was analyzed with XPS (Table S1, SI). The larger O/N ratio (2.532) of the HRM^{SW30} membrane compared with the pristine (1.490) and the SRM^{SW30} (1.489) indicates the generation of excess oxygenous groups and/or the cleavage of amide bond forming -COO moieties in the active layer. The more oxygenous groups and/or decreased cross-linking degree of the HRM^{SW30} membrane are likely responsible for its enhanced water permeability and high NaCl rejection (Figure 1). Additionally, the significantly lower surface water contact angle (Figure S8, SI) and more negative surface charge (Figure S9, SI) observed for the HRM^{SW30} should also be ascribed to the oxidation. The elemental composition of the SRM^{SW30} membrane remained unchanged and the water contact angle and surface charge slightly decreased as compared with the pristine membrane. The difference in surface property of the HRM^{SW30} and SRM^{SW30} membranes implies different reactivity of $HO^{\bullet}$ and $SO_4^{\bullet-}$ with polyamide, which will be addressed in the next section.

Reaction of Radicals with Model Polyamide Monomer. Benzanilide (BA) has a similar chemical structure to the primary moiety of polyamide and has been widely used as a molecular polyamide model monomer to study the reactivity of polyamide with oxidants (e.g., free chlorine) in the literature.[44, 45] It was selected here to investigate the reaction mechanism between polyamide and oxidant species generated in the PDS solution. Initially, experiments were conducted at pH 4 and 10

under PDS/BA molar ratios of 3:1, 5:1, and 10:1, respectively (Figure 3a and 3b). Hydrolysis of BA was not observed at the two pHs. PDS at room temperature was unreactive towards BA in water (Figure S10, SI). BA clearly reacted with the oxidant species generated from PDS decomposition at pH 4 and 10, and the reaction rate accelerated with increasing PDS dosage. BA degraded continuously with time at pH 4 and disappeared in 24 h at the PDS/BA molar ratio of 10:1. In contrast, only 42% BA degraded at pH 10 at the same PDS dosage and reaction time. Even when the reaction was extended to 48 h, 51% BA was still detected as residual at pH 10. The PDS decomposed at the two pHs were 48.6% and 49.7%, respectively, after 48 h reaction. The lower BA degradation rate at pH 10 probably is due to the competitive consumption of $HO^{\bullet}$ by BA transformation products. The relatively fast and continuous BA removal at pH 4 demonstrates higher selectivity of $SO_4^{\bullet-}$ than $HO^{\bullet}$ in reaction with BA. The different selectivity of the two radicals was also observed in the degradation of some water pollutants.[46] This result is consistent with the stronger PDS dosage-relevance of the membrane modification at pH 4 than that at pH 10 (Figure 1). After reaction at pH 4, clustered aggregates were generated in the BA solution, which is distinct from the transparent solution observed after the reaction at pH 10 (photos in Figure 3a and 3b). These results clearly show that reactions that dominated BA degradation at pH 4 and 10 are different.

Figure 3

The formula and plausible molecular structures of BA transformation products are provided in Figures S11 and S12 (SI) and summarized in Tables S2 and S3 (SI). At pH 4, benzamide, diphenol-BA, and benzoquinone-BA biphenyl were detected after oxidation at the PDS/BA molar ratio of 5:1. In fact, under the $SO_4^{\bullet-}$-dominated reaction condition, aromatic radical cations such as $BA^{\bullet+}$ and $benzene^{\bullet+}$ may form via electron abstraction, followed by a rearrangement to undergo side-chain oxidation, resulting in the conversion to phenols or biphenyls.[24, 47] Then, the phenols undergo oxidative polymerization with $BA^{\bullet+}$ to form oligomers.[48-50] As the PDS/BA molar ratio was raised to 10:1,

isomers of BA dimers were detected, which are characteristic products in $SO_4^{\bullet-}$ oxidation.[24] Additionally, the aggregates formed under pH 4 were collected through centrifugation and characterized with FTIR (Figure S13, SI). The characteristic peaks of amide, i.e., N-H at 3344 cm^{-1}, C=O (amide I) at 1655 cm^{-1}, and N-H (amide II) at 1533 cm^{-1}, were consistent with those of the BA monomer. The multiple peaks of aromatic rings at the wavenumber of 1250–1600 cm^{-1} merged into wider ones after reaction, which could be ascribed to the polymerization of BA and agrees with the emergence of $\pi \rightarrow \pi^*$ satellite peak observed in the C 1s XPS spectrum (Figure 2d). The intense peak at 817 cm^{-1} comes from the para-orientation of aromatic rings,[51, 52] indicating that the oxidative polymerization of BA forms mainly through para-substitution.

Oxidative hydroxylation of BA was the major reaction occurring at pH 10 at the PDS/BA molar ratio of 5:1.[24] Further increasing the ratio to 10:1, BA transformation products were merely detected by QTof, suggesting that the hydroxylated transformation products further degraded into small molecules. Then, the products were derivatized with methanol under acidic conditions and analyzed with GC/MS (Figure S14 and Table S4, SI). Benzoic acid and nitrobenzene were consequently detected. Nitrobenzene could be the oxidation product of aniline by $HO^{\bullet}$ in the thermal activated PDS solution.[53] This result suggests that $HO^{\bullet}$ oxidation possibly induced the cleavage of the amide bond (N-CO) of BA. Whereas for the $SO_4^{\bullet-}$-dominated oxidation at pH 4, neither aniline nor nitrobenzene was detected. BA dimer and benzoquinone, the characteristic transformation products observed at pH 4, were not detected after the oxidation at pH 10. Plausible reaction pathways of the BA monomer under thermal-activated PDS at pH 4 and 10 are proposed in Figure 3c. Based on the transformation product identification and the one order of magnitude higher reaction rate constant of $HO^{\bullet}$ with benzamide than that of $SO_4^{\bullet-}$ (2.6×10^9 $M^{-1}s^{-1}$ vs. 1.9×10^8 $M^{-1}s^{-1}$)[54], we can conclude that the reaction of BA was governed by $HO^{\bullet}$ and $SO_4^{\bullet-}$, respectively, at pH 10 and 4. In addition, even $SO_4^{\bullet-}$ exists at pH 10, its interaction with polyamide membrane (with pK_a ~5.2[55]) is not favorable due to

electrostatic repulsion. The swelling behavior of polyamide at pH 10 due to the increased electrostatic repulsion between the dissociated carboxylic groups may increase the interaction of radicals.[56] Besides, the reaction rate constants of $HO^{\bullet}$ towards aniline (1.4×10^{10} $M^{-1}s^{-1}$) and benzoic acid (4.2×10^{9} $M^{-1}s^{-1}$), the ionized moieties in the polyamide layer, are higher than those of $SO_4^{\bullet-}$ (7.7×10^{9} $M^{-1}s^{-1}$ and 1.2×10^{9} $M^{-1}s^{-1}$).[22, 57, 58] However, the modification was more effective at pH 4 than pH 10 (Figure 1). It is consistent with the reaction rates of $SO_4^{\bullet-}$ and $HO^{\bullet}$ with BA, the primary moiety in the polyamide layer (Figures 3a and 3b). Hence, we can speculate that the major modification reaction occurred between radicals and the BA moiety, which presents minor changes in speciation in the pH range of 4–10 (pK_a = 16.53)[59]. Therefore, the differences in the physicochemical property, as well as the filtration performance of the HRM^{SW30} and SRM^{SW30} membranes, can be ascribed to the different reaction pathways of $HO^{\bullet}$ and $SO_4^{\bullet-}$ towards polyamide.

Correlation between Membrane Surface Property and Performance. As discussed above, PDS thermally activated under acidic or base conditions modified the polyamide membrane through different mechanisms. The modification at pH 10 broke the amide bonds of the polyamide layer and endowed the HRM^{SW30} membrane with excess hydroxyl, carboxyl, and nitro groups. This change of surface chemistry improved hydrophilicity (Figure S8, SI), enhanced surface charge (Figure S9, SI), and slightly increased the estimated pore size (Table S5, r_p = 0.3648 nm) as compared with the pristine SW30 membrane (r_p = 0.3504 nm), which contributed to the significant increase of water permeability of the membrane (Figure 1). The carboxyl groups on the HRM^{SW30} membrane surface were further quantified with a silver-binding method (Table S6, SI). The carboxyl group density of the HRM^{SW30} membrane was notably higher than the pristine and SRM^{SW30} membrane (20.40, 11.86, and 13.65 sites/nm^2, respectively). The formation of nitro groups was not observed in the XPS N1s spectrum (~ 406 eV) (Figure S7, SI), which is likely due to the relatively low detection depth of XPS measurement (a few nanometers). $SO_4^{\bullet-}$ initiated the redox polymerization of polyamide associated

with bond cleavage (HN-ring) and the following formation of biphenyl structures, strengthening salt rejection by steric exclusion (r_p: 0.3363 vs. 0.3504 nm), thereby exhibiting high salt rejection in wide pH (pH 2–9, Figure 4a and Table S7) and salinity (Figure S15) ranges. Besides, the introduced hydroquinone structure may contribute to the improved hydrophilicity and permeability of the SRM^{SW30} membrane (Figures 1 and S8).

Figure 4

The improvement in surface properties such as hydrophilicity induced by hydroxyl and carboxyl groups enhanced the fouling resistance of HRM^{SW30} and SRM^{SW30} membranes to organic foulants (e.g., humic substances). The water flux over time, normalized by the initial value (setting at 20.0 ± 0.5 L m^{-2} h^{-1} by adjusting the hydraulic pressure), is shown in Figure 4b. The HRM^{SW30} and SRM^{SW30} membranes exhibited slightly less flux decline (~10.5%) compared to the pristine membrane (13.8% reduction) after the 12 h organic fouling experiment. Also, the permeation resistance of the membrane matrix (R_M) and fouling layer (R_{HA}) all decreased after modification at pH 4 or 10 (Figure 4c). The hydroxyl and carboxyl groups on the modified membrane surface favor the formation of hydration shells at the membrane/water interface, hence hindering the adsorption of HA on the membrane surface. The lower HA mass desorbed from the modified membrane surface after the fouling test further confirms that less HA was adsorbed onto the surface of the modified membranes (Figure 4c).

Compared with the pristine membrane, both the HRM^{SW30} and SRM^{SW30} membranes showed higher salt rejection after chlorine exposure at various pH (Figure 4d). The conversion of the terminal -NH_2 groups to -NO_2 on the HRM^{SW30} membrane transformed the electronegative nitrogen (electron-donating) to electropositive (electron-withdrawing), thus reducing the chlorination reaction of residual amino groups.[60]. Additionally, nitro groups deactivated the aromatic rings against electrophilic chlorination, with extended Huckel atomic charge being decreased from -0.179 and -0.203 to -0.05 (Figure 5a). The SRM^{SW30} membrane possessed significantly improved salt rejection even after severe

chlorine exposure at pH 4. The enhanced chlorine resistance of the SRM^{SW30} membrane may be ascribed to the synergistic effect of the denser active layer and slightly reduced charge of the aromatic ring due to the formation of biphenyl- and benzoquinone-polyamide structures (Figure 5a).

Figure 5

As illustrated in Figure 5b, the polyamide membranes modified through radical oxidation possessed characteristic functional groups (HRM: -OH, -COOH, $-NO_2$; SRM: -OH, biphenyl- and benzoquinone-) and showed comprehensively improved performance in terms of water flux and fouling- and chlorine-resistances while maintaining high salt rejection. Considering the higher reaction selectivity (lower PDS doses), higher salt rejection over wide pH and salinity ranges, and more enhanced chlorine resistance of the SRM membrane, modification in acidic PDS solution governed by $SO_4^{\bullet-}$ is more promising. Besides, moderate $SO_4^{\bullet-}$-based modification could maintain the integrity of the polyamide structure. The current study mainly focused on revealing the mechanisms of performance enhancement from the viewpoint of surface physicochemical properties. Potential variations of the structural homogeneity such as internal morphology, density, and distribution of functional groups in the active layer induced by oxidative modification may also affect the membrane performance[61], which will be investigated in future studies.

Environmental implications.

This study demonstrates that radical oxidation is a facile and effective modification strategy for aromatic polyamide RO membrane. The pH of the PDS solution, which governs the speciation of radicals ($HO^{\bullet}$ and $SO_4^{\bullet-}$), distinctly determines the modification mechanism and surface properties of the modified membranes. By incorporating hydroxyl, carboxyl, and nitro functional groups, or benzoquinone and multi-phenyl structures, the water permeability, anti-fouling, and anti-chlorine capabilities of the polyamide membrane could be significantly improved without severely sacrificing salt rejection. The chemical resistance of the HRM and SRM membranes for a 6-round alternate

386 acid/base cleaning was demonstrated in Figure S16 (SI) and indicated the performance stability of the
387 oxidatively modified membranes. Additionally, the HRM and SRM membranes exhibited different
388 NaCl rejections at various solution salinities (Figure S15, SI) due to variations in surface properties
389 (i.e., surface charge and pore size). Specifically, the HRM membrane with increased surface charge
390 had similar NaCl rejection with the pristine membrane at mild salinity (≤ 100 mM NaCl, Table S8,
391 SI). However, the NaCl rejection of the HRM membrane was lower than the pristine as the salinity
392 further increased to 200 and 300 mM due to the charge screening effect. In contrast, the solution
393 salinity had less impact on the NaCl rejection of the SRM membrane, and size exclusion was supposed
394 to play an important role in the solute rejection. Therefore, the oxidatively modified membranes,
395 especially the SRM membrane with significantly improved filtration performance, can be potentially
396 applied in freshwater purification, brackish water desalination, and wastewater reuse. Besides, the
397 oxidative modification applied in the study can also improve the water permeability of brackish water
398 RO membrane, e.g., the BW30 membrane (Figure S17, SI). The specific surface properties induced
399 by oxidation will expand the prospects of novel materials for energy-efficient water purification.

400 This study also provides new insights into the development of sustainable oxidation-combined
401 membrane processes. The performance of TFC membranes will vary regarding the type and
402 concentration of oxidants introduced. Therefore, the oxidation processes generating various reactive
403 oxygen species (e.g., $HO^{\bullet}$ or $SO_4^{\bullet-}$) should be carefully designed for target treatments. For example,
404 for the treatment with low scaling potential such as RO for water reuse, combining $SO_4^{\bullet-}$-oxidation of
405 a moderate dosage may endow the membrane with high water permeance and antifouling properties.
406 Otherwise, the non-selective $HO^{\bullet}$ may cause the failure of the TFC membrane eventually and have
407 detrimental effects on the rejection of solutes, especially for neutral small organics. For novel
408 catalytic/electric membrane materials and oxidation-combined membrane processes that possibly
409 generate $HO^{\bullet}$ or $SO_4^{\bullet-}$, the negative impacts of secondary radical species (e.g., $Cl^{\bullet}$ and $Cl_2^{\bullet-}$) that

derived from halide ions (e.g., Cl^-) in the water matrix on membrane performance should be avoided (Figure S18, SI).[62] Specifically, the halide ions in the presence of $SO_4^{\bullet-}$ have more detrimental effects on the permselectivity of the TFC membrane.

ACKNOWLEDGMENTS

We acknowledge the support from the National Key Research and Development Program of China (grant 2021YFC3201401). We also thank for the support from the National Natural Science Foundation of China (grant 52000175).

SUPPORTING INFORMATION

The Supporting Information is available free of charge on the ACS Publications website.

Detailed information of membrane performance and fouling tests (Text S1), carboxyl group area density measurement (Text S2), effective pore size measurement (Text S3), setting for QTof mass system (Text S4), methylation and setting for GC-MS analysis (Text S5), degradation of 2,4-DCP by thermally activated PDS (Figure S1), decomposition of PDS and PMS (Figure S2), effect of background condition on RO membrane performances (Figure S3), photos of membranes (Figure S4), active layer thickness (Figure S5), ATR-FTIR spectra (Figure S6), N 1s XPS spectra (Figure S7), water contact angle (Figure S8), and surface zeta potential (Figure S9) of the membranes before and after modification, BA degradation at room temperature (Figure S10), QTof IDA survey of the BA degradation products (Figure S11), IDA TOf MSMS spectra of the BA degradation products (Figure S12), FTIR of the aggregated product (Figure S13), GC/MS analysis of the BA degradation products (Figure S14), NaCl rejection at different solution salinities (Figure S15), chemical resistance (Figure S16), modification of BW30 membranes (Figure S17), effect of halide ions (Figure S18), XPS surface elemental composition (Table S1), formular and proposed structure of the BA degradation products (Tables S2-S4), rejection of tracers and estimated average pore radius (Table S5), surface carboxyl group areal density of the membranes (Table S6), solute rection at pH 2 and 3 (Table S7), and typical water salinity (Table S8).

REFERENCES

1. Werber, J. R.; Osuji, C. O.; Elimelech, M., Materials for next-generation desalination and water purification membranes. *Nat. Rev. Mater.* **2016,** *1*, (5).
2. Elimelech, M.; Phillip, W. A., The future of seawater desalination: Energy, technology, and the environment. *Science* **2011,** *333*, (6043), 712-717.
3. Qasim, M.; Badrelzaman, M.; Darwish, N. N.; Darwish, N. A.; Hilal, N., Reverse osmosis desalination: A state-of-the-art review. *Desalination* **2019,** *459*, 59-104.
4. Lu, X.; Elimelech, M., Fabrication of desalination membranes by interfacial polymerization: History, current efforts, and future directions. *Chem. Soc. Rev.* **2021,** *50*, (11), 6290-6307.
5. Cohen-Tanugi, D.; McGovern, R. K.; Dave, S. H.; Lienhard, J. H.; Grossman, J. C., Quantifying the potential of ultra-permeable membranes for water desalination. *Energy Environ. Sci.* **2014,** *7*, (3), 1134-1141.
6. Ritt, C. L.; Werber, J. R.; Wang, M.; Yang, Z.; Zhao, Y.; Kulik, H. J.; Elimelech, M., Ionization behavior of nanoporous polyamide membranes. *Proc. Natl. Acad. Sci. U. S. A.* **2020,** *117*, (48), 30191-30200.
7. Park, H. B.; Kamcev, J.; Robeson, L. M.; Elimelech, M.; Freeman, B. D., Maximizing the right stuff: The trade-off between membrane permeability and selectivity. *Science* **2017,** *356*, (6343).

8. Li, W.; Yang, Z.; Liu, W.; Huang, Z.; Zhang, H.; Li, M.; Ma, X.; Tang, C.; Xu, Z., Polyamide reverse osmosis membranes containing 1D nanochannels for enhanced water purification. *J. Membr. Sci.* **2021,** *618*, 118681.
9. Dong, H.; Zhao, L.; Zhang, L.; Chen, H.; Gao, C.; Winston Ho, W. S., High-flux reverse osmosis membranes incorporated with NaY zeolite nanoparticles for brackish water desalination. *J. Membr. Sci.* **2015,** *476*, 373-383.
10. Wang, J.; Wang, Z.; Wang, J. X.; Wang, S. C., Improving the water flux and bio-fouling resistance of reverse osmosis (RO) membrane through surface modification by zwitterionic polymer. *J. Membr. Sci.* **2015,** *493*, 188-199.
11. Hu, Y.; Lu, K.; Yan, F.; Shi, Y.; Yu, P.; Yu, S.; Li, S.; Gao, C., Enhancing the performance of aromatic polyamide reverse osmosis membrane by surface modification via covalent attachment of polyvinyl alcohol (PVA). *J. Membr. Sci.* **2016,** *501*, 209-219.
12. Rho, H.; Im, S. J.; Alrehaili, O.; Lee, S.; Jang, A.; Perreault, F.; Westerhoff, P., Facile surface modification of polyamide membranes using UV-photooxidation improves permeability and reduces natural organic matter fouling. *Environ. Sci. Technol.* **2021,** *55*, (10), 6984-6994.
13. Bi, Y. Q.; Han, B. R.; Zimmerman, S.; Perreault, F.; Sinha, S.; Westerhoff, P., Four release tests exhibit variable silver stability from nanoparticle-modified reverse osmosis membranes. *Water Res.* **2018,** *143*, 77-86.
14. Ghosh, A. K.; Jeong, B.-H.; Huang, X.; Hoek, E. M. V., Impacts of reaction and curing conditions on polyamide composite reverse osmosis membrane properties. *J. Membr. Sci.* **2008,** *311*, (1-2), 34-45.
15. Zhan, Z.; Xu, Z.; Zhu, K.; Xue, S.; Ji, C.; Huang, B.; Tang, C. Y.; Tang, Y., Superior nanofiltration membranes with gradient cross-linked selective layer fabricated via controlled hydrolysis. *J. Membr. Sci.* **2020,** *604*, 118067.
16. Zhang, R.; Su, S.; Gao, S.; Tian, J., Reconstruction of the polyamide film in nanofiltration membranes via the post-treatment with a ternary mixture of ethanol-water-NaOH: Mechanism and effect. *Desalination* **2021,** *519*, 115317.
17. Verbeke, R.; Eyley, S.; Szymczyk, A.; Thielemans, W.; Vankelecom, I. F. J., Controlled chlorination of polyamide reverse osmosis membranes at real scale for enhanced desalination performance. *J. Membr. Sci.* **2020,** *611*, 118400.
18. Do, V. T.; Tang, C. Y.; Reinhard, M.; Leckie, J. O., Effects of chlorine exposure conditions on physiochemical properties and performance of a polyamide membrane--mechanisms and implications. *Environ. Sci. Technol.* **2012,** *46*, (24), 13184-13192.
19. Bing, S.; Wang, J.; Xu, H.; Zhao, Y.; Zhou, Y.; Zhang, L.; Gao, C.; Hou, L. a., Polyamide thin-film composite membrane modified with persulfate for improvement of perm-selectivity and chlorine-resistance. *J. Membr. Sci.* **2018,** *555*, 318-326.
20. Liu, N.; Sijak, S.; Zheng, M.; Tang, L.; Xu, G.; Wu, M., Aquatic photolysis of florfenicol and thiamphenicol under direct UV irradiation, UV/H2O2 and UV/Fe(II) processes. *Chem. Eng. J* **2015,** *260*, 826-834.
21. Gijsman, P.; Meijers, G.; Vitarelli, G., Comparison of the UV-degradation chemistry of polypropylene, polyethylene, polyamide 6 and polybutylene terephthalate. *Polym. Degrad. Stabil.* **1999,** *65*, (3), 433-441.
22. Liang, C.; Su, H.-W., Identification of sulfate and hydroxyl radicals in thermally activated persulfate. *Ind. Eng. Chem. Res.* **2009,** *48*, (11), 5558-5562.
23. Guan, Y. H.; Ma, J.; Li, X. C.; Fang, J. Y.; Chen, L. W., Influence of pH on the formation of sulfate and hydroxyl radicals in the UV/peroxymonosulfate system. *Environ. Sci. Technol.* **2011,** *45*, (21), 9308-14.
24. Lee, J.; von Gunten, U.; Kim, J.-H., Persulfate-based advanced oxidation: Critical assessment of opportunities and roadblocks. *Environ. Sci. Technol.* **2020,** *54*, (6), 3064-3081.
25. Song, W., Nanofiltration of natural organic matter with H2O2/UV pretreatment: Fouling mitigation and membrane surface characterization. *J. Membr. Sci.* **2004,** *241*, (1), 143-160.
26. Bai, L. M.; Liu, Z. H.; Wang, H. R.; Li, G. B.; Liang, H., Fe(II)-activated peroxymonosulfate coupled with nanofiltration removes natural organic matter and sulfamethoxazole in natural surface water: Performance and mechanisms. *Sep. Purif. Technol.* **2021,** *274*, 119088.
27. Janssens, R.; Cristovao, M. B.; Bronze, M. R.; Crespo, J. G.; Pereira, V. J.; Luis, P., Coupling of nanofiltration and UV, UV/TiO2 and UV/H2O2 processes for the removal of anti-cancer drugs from real secondary wastewater

effluent. *J. Environ. Chem. Eng.* **2019,** *7*, (5), 103351.
28. Kim, S. H.; Kwak, S.-Y.; Sohn, B.-H.; Park, T. H., Design of TiO2 nanoparticle self-assembled aromatic polyamide thin-film-composite (TFC) membrane as an approach to solve biofouling problem. *J. Membr. Sci.* **2003,** *211*, (1), 157-165.
29. Kwak, S. Y.; Kim, S. H.; Kim, S. S., Hybrid organic/inorganic reverse osmosis (RO) membrane for bactericidal anti-fouling. 1. Preparation and characterization of TiO2 nanoparticle self-assembled aromatic polyamide thin-film-composite (TFC) membrane. *Environ. Sci. Technol.* **2001,** *35*, (11), 2388-2394.
30. Liang, C.; Bruell, C. J.; Albert, M. F.; Cross, P. E.; Ryan, D. K., Evaluation of reverse osmosis and nanofiltration for in situ persulfate remediated groundwater. *Desalination* **2007,** *208*, (1-3), 238-259.
31. Ling, R.; Yu, L.; Pham, T. P. T.; Shao, J.; Chen, J. P.; Reinhard, M., The tolerance of a thin-film composite polyamide reverse osmosis membrane to hydrogen peroxide exposure. *J. Membr. Sci.* **2017,** *524*, 529-536.
32. Johnson, R. L.; Tratnyek, P. G.; Johnson, R. O. B., Persulfate persistence under thermal activation conditions. *Environ. Sci. Technol.* **2008,** *42*, (24), 9350-9356.
33. Liang, C. J.; Huang, C. F.; Mohanty, N.; Kurakalva, R. M., A rapid spectrophotometric determination of persulfate anion in ISCO. *Chemosphere* **2008,** *73*, (9), 1540-1543.
34. Chen, D.; Werber, J. R.; Zhao, X.; Elimelech, M., A facile method to quantify the carboxyl group areal density in the active layer of polyamide thin-film composite membranes. *J. Membr. Sci.* **2017,** *534*, 100-108.
35. Wang, P.; Li, J.; Zhang, X.; Lu, X.; Liu, Q.; Zhang, T.; Cheng, W.; Ma, J., Utilization of bidirectional cation transport in a thin film composite membrane: Selective removal and reclamation of ammonium from synthetic digested sludge centrate via an osmosis-distillation hybrid membrane process. *Environ. Sci. Technol.* **2020,** *54*, (16), 10313-10322.
36. Xie, M.; Nghiem, L. D.; Price, W. E.; Elimelech, M., Comparison of the removal of hydrophobic trace organic contaminants by forward osmosis and reverse osmosis. *Water Res.* **2012,** *46*, (8), 2683-92.
37. Kwon, Y.-N.; Leckie, J. O., Hypochlorite degradation of crosslinked polyamide membranes: II. Changes in hydrogen bonding behavior and performance. *J. Membr. Sci.* **2006,** *282*, (1-2), 456-464.
38. Tang, C. Y.; Kwon, Y.-N.; Leckie, J. O., Effect of membrane chemistry and coating layer on physiochemical properties of thin film composite polyamide RO and NF membranes. *Desalination* **2009,** *242*, (1-3), 149-167.
39. Shen, L.; Wang, F.; Tian, L.; Zhang, X.; Ding, C.; Wang, Y., High-performance thin-film composite membranes with surface functionalization by organic phosphonic acids. *J. Membr. Sci.* **2018,** *563*, 284-297.
40. Yao, Z.; Guo, H.; Yang, Z.; Qing, W.; Tang, C. Y., Preparation of nanocavity-contained thin film composite nanofiltration membranes with enhanced permeability and divalent to monovalent ion selectivity. *Desalination* **2018,** *445*, 115-122.
41. Buechner, C.; Gericke, S. M.; Trotochaud, L.; Karslioglu, O.; Raso, J.; Bluhm, H., Quantitative characterization of a desalination membrane model system by X-ray photoelectron spectroscopy. *Langmuir* **2019,** *35*, (35), 11315-11321.
42. Kwan, Y. C. G.; Ng, G. M.; Huan, C. H. A., Identification of functional groups and determination of carboxyl formation temperature in graphene oxide using the XPS O 1s spectrum. *Thin Solid Films* **2015,** *590*, 40-48.
43. Inagaki, N.; Narushima, K.; Lim, S. K., Effects of aromatic groups in polymer chains on plasma surface modification. *J. Appl. Polym. Sci.* **2003,** *89*, (1), 96-103.
44. Huang, K.; Reber, K. P.; Toomey, M. D.; Haflich, H.; Howarter, J. A.; Shah, A. D., Reactivity of the polyamide membrane monomer with free chlorine: Reaction kinetics, mechanisms, and the role of chloride. *Environ. Sci. Technol.* **2019,** *53*, (14), 8167-8176.
45. Soice, N. P.; Maladono, A. C.; Takigawa, D. Y.; Norman, A. D.; Krantz, W. B.; Greenberg, A. R., Oxidative degradation of polyamide reverse osmosis membranes: Studies of molecular model compounds and selected membranes. *J. Appl. Polym. Sci.* **2003,** *90*, (5), 1173-1184.
46. Nihemaiti, M.; Miklos, D. B.; Hubner, U.; Linden, K. G.; Drewes, J. E.; Croue, J. P., Removal of trace organic chemicals in wastewater effluent by UV/H2O2 and UV/PDS. *Water Res.* **2018,** *145*, 487-497.

47. Caregnato, P.; Gara, P. M.; Bosio, G. N.; Gonzalez, M. C.; Russo, N.; Michelini Mdel, C.; Martire, D. O., Theoretical and experimental investigation on the oxidation of gallic acid by sulfate radical anions. *J. Phys. Chem. A.* **2008,** *112*, (6), 1188-1194.
48. Bláha, M.; Trchová, M.; Bober, P.; Morávková, Z.; Prokeš, J.; Stejskal, J., Polyaniline: Aniline oxidation with strong and weak oxidants under various acidity. *Mater. Chem. Phys.* **2017,** *194*, 206-218.
49. Janošević, A.; Ćirić-Marjanović, G.; Šljukić Paunković, B.; Pašti, I.; Trifunović, S.; Marjanović, B.; Stejskal, J., Simultaneous oxidation of aniline and tannic acid with peroxydisulfate: Self-assembly of oxidation products from nanorods to microspheres. *Synthetic Met.* **2012,** *162*, (9-10), 843-856.
50. Ćirić-Marjanović, G.; Trchová, M.; Stejskal, J., Theoretical study of the oxidative polymerization of aniline with peroxydisulfate: Tetramer formation. *Int. J. Quantum. Chem.* **2008,** *108*, (2), 318-333.
51. Yu, C.; WeiPing, L.; YanChun, Y.; YanWen, G.; TianWei, W.; Yi-Fan, X., The novel route to prepare immobilized macrocyclic compound on 6-OH of chitosan with good solubility and prime study on its applications. *Mol. Cryst. Liq. Cryst.* **2014,** *604*, (1), 202-212.
52. Jiang, D. D.; Yao, Q.; McKinney, M. A.; Wilkie, C. A., TGA/FTIR studies on the thermal degradation of some polymeric sulfonic and phosphonic acids and their sodium salts. *Polym. Degrad. Stabil.* **1999,** *63*, (3), 423-434.
53. Xie, X.; Zhang, Y.; Huang, W.; Huang, S., Degradation kinetics and mechanism of aniline by heat-assisted persulfate oxidation. *J. Environ. Sci.* **2012,** *24*, (5), 821-826.
54. Wojnárovits, L.; Takács, E., Rate constants of sulfate radical anion reactions with organic molecules: A review. *Chemosphere* **2019,** *220*, 1014-1032.
55. Lu, X.; Boo, C.; Ma, J.; Elimelech, M., Bidirectional diffusion of ammonium and sodium cations in forward osmosis: role of membrane active layer surface chemistry and charge. *Environ. Sci. Technol.* **2014,** *48*, (24), 14369-76.
56. Wang, J.; Mo, Y.; Mahendra, S.; Hoek, E. M. V., Effects of water chemistry on structure and performance of polyamide composite membranes. *J. Membr. Sci.* **2014,** *452*, 415-425.
57. Yuan, Y.; Luo, T.; Xu, J.; Li, J.; Wu, F.; Brigante, M.; Mailhot, G., Enhanced oxidation of aniline using Fe(III)-S(IV) system: Role of different oxysulfur radicals. *Chem. Eng. J.* **2019,** *362*, 183-189.
58. Christensen, H., Pulse radiolysis of aqueous solutions of aniline and substituted anilines. *Int. J. Radiat. Phys. Chem.* **1972,** *4*, (3), 311-333.
59. Yam, V. W.-W.; Kai, A. S.-F., Synthesis and optical sensing properties of a boronic acid appended rhenium(I) complex for sugar. *Chem. Commun* **1998**, (1), 109-110.
60. Yao, Y.; Zhang, W.; Du, Y.; Li, M.; Wang, L.; Zhang, X., Toward enhancing the chlorine resistance of reverse osmosis membranes: An effective strategy via an end-capping technology. *Environ. Sci. Technol.* **2019,** *53*, (3), 1296-1304.
61. Culp, T. E.; Khara, B.; Brickey, K. P.; Geitner, M.; Zimudzi, T. J.; Wilbur, J. D.; Jons, S. D.; Roy, A.; Paul, M.; Ganapathysubramanian, B.; Zydney, A. L.; Kumar, M.; Gomez, E. D., Nanoscale control of internal inhomogeneity enhances water transport in desalination membranes. *Science* **2021,** *371*, (6524), 72-75.
62. Valentino, L.; Renkens, T.; Maugin, T.; Croué, J.-P.; Mariñas, B. J., Changes in physicochemical and transport properties of a reverse osmosis membrane exposed to chloraminated seawater. *Environ. Sci. Technol.* **2015,** *49*, (4), 2301-2309.

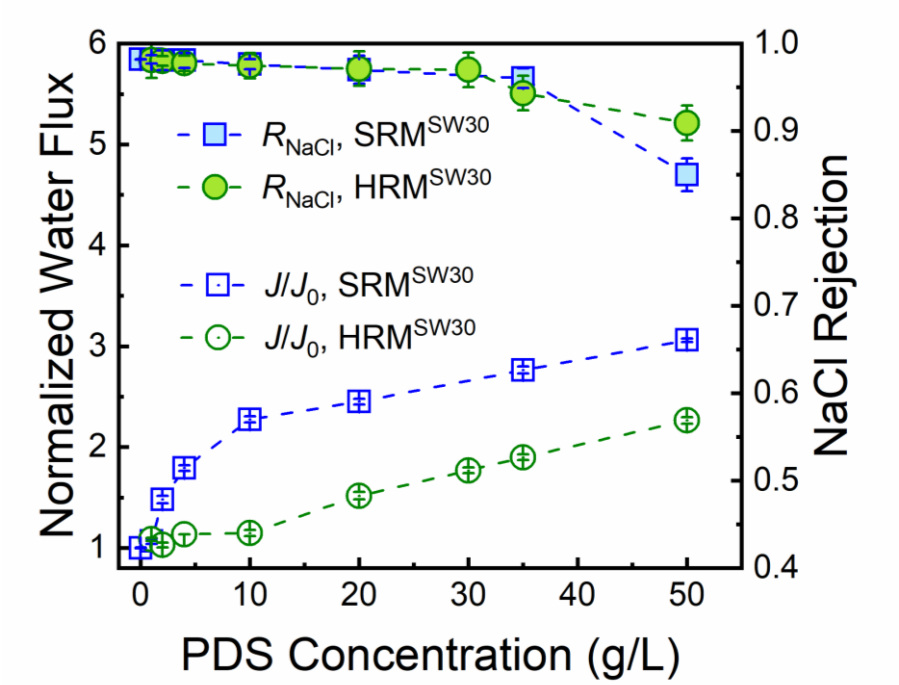

Figure 1. Normalized water flux and salt rejection of the polyamide SW30 membrane before and after oxidative modification. The PDS dose was 1–50 g/L for the modification of SW30. The water flux of the pristine SW30 membrane was 17.50 ± 0.20 L m^{-2} h^{-1} at hydraulic pressures of 14 bar.

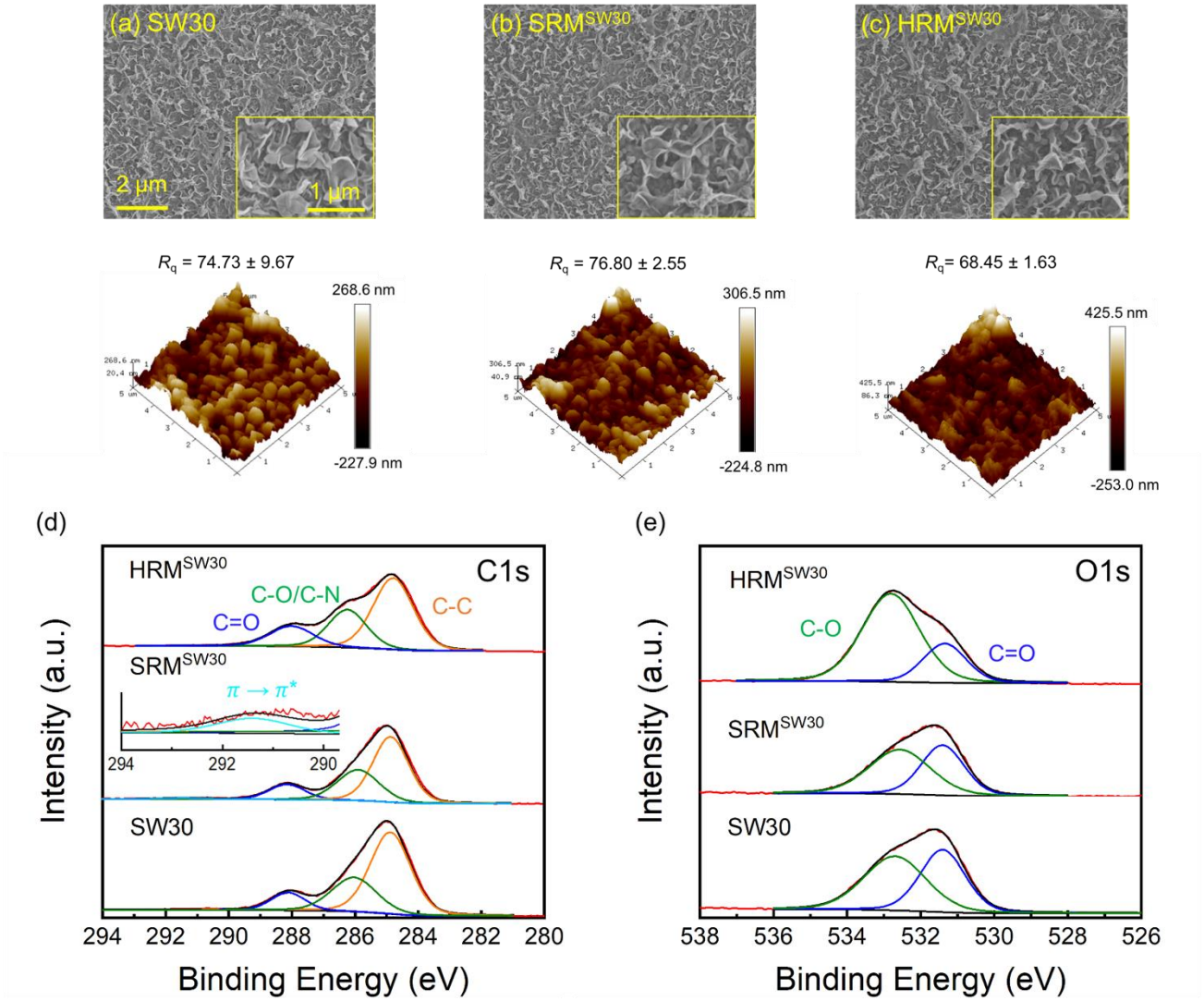

Figure 2. Surface characterization for the pristine and modified SW30 membranes. SEM (scale bar = 2 μm) and AFM morphologies of the SW30 (a), SRM^{SW30} (b), and HRM^{SW30} (c) membranes. The roughness values (R_q) of the SRM and HRM membranes are significantly different from each other (Student's *t*-test, n = 3, $p < 0.05$), while the roughness of the pristine SW30 shows a relatively large deviation which may be due to samples discrepancy. XPS spectra of C1s (d) and O1s (e) for the pristine and modified SW30 membranes. The SW30 membrane was modified by using 4 g/L PDS at pH 4 (SRM^{SW30}) or 30 g/L PDS at pH 10 (HRM^{SW30}).

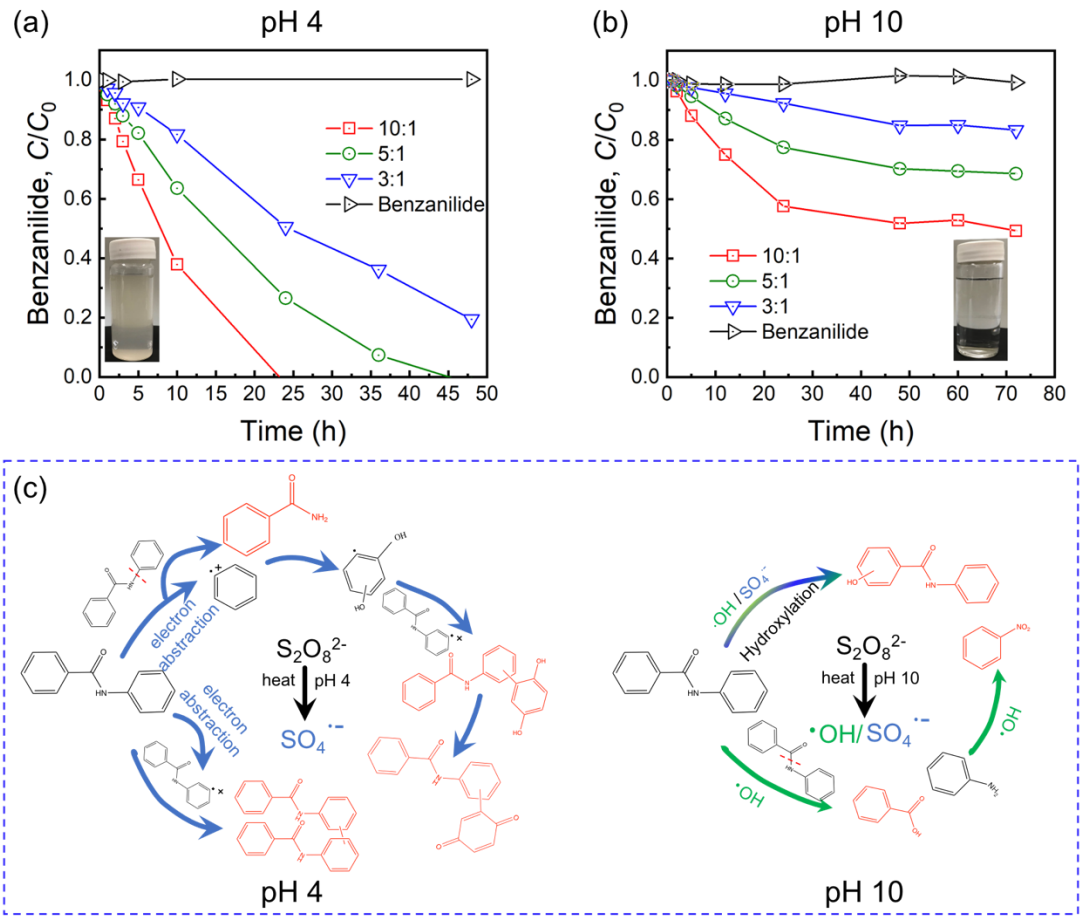

Figure 3. Degradation of BA monomer by PDS at pH 4 (a) and pH 10 (b). Various concentrations of PDS (600, 1000, and 2000 μM) were used to react with BA (200 μM) at molar ratios of 3:1, 5:1, and 10:1, respectively. Plausible transformation products and reaction pathways of BA with PDS at pH 4 and pH 10 (c). The proposed structures of BA transformation products were analyzed by QTof mass spectrometer and GC/MS (marked in red).

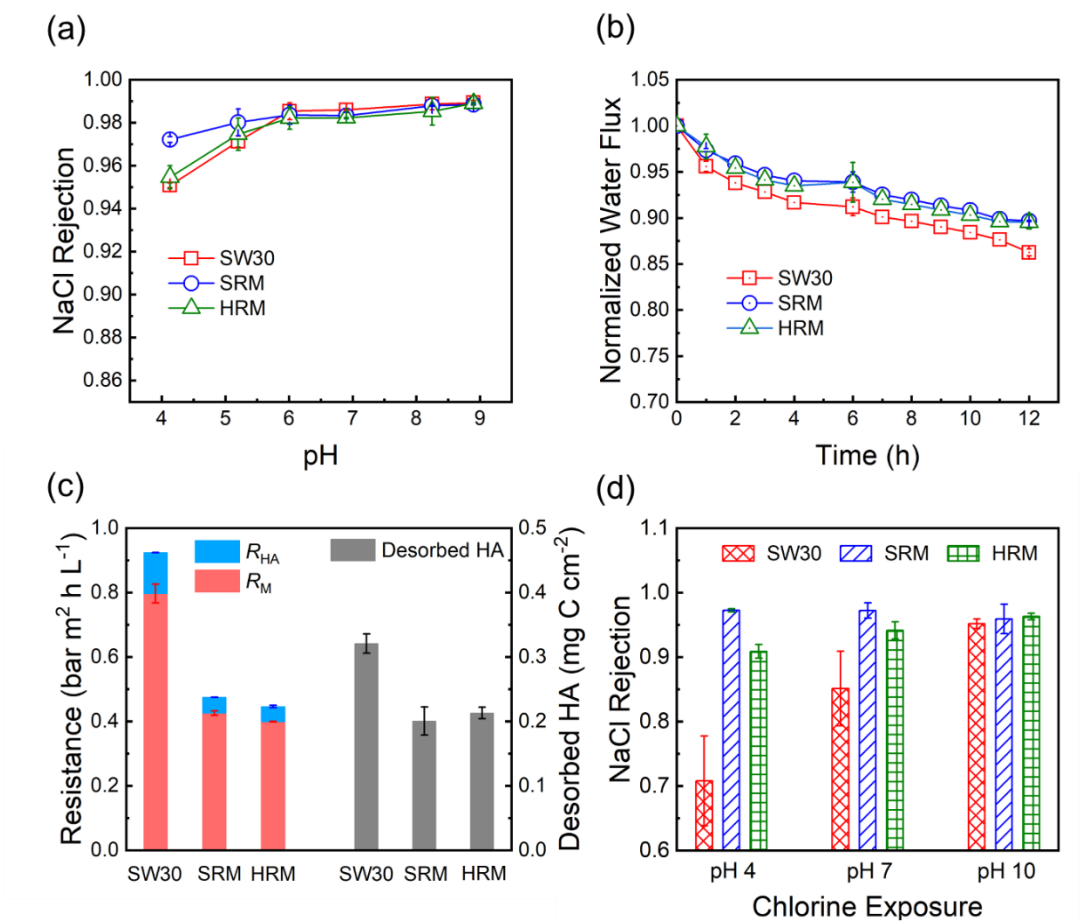

Figure 4. (a) NaCl rejections of the pristine and modified SW30 membranes at different solution pH (4.0–9.5). (b) Water flux variation of the membranes in the presence of HA. The initial water flux was set at 20.0 ± 1.0 L m^{-2} h^{-1} by adjusting the hydraulic pressure. The final water flux values of the SRM and HRM membranes are significantly different from the value of the pristine SW30 (Student's *t*-test, $n = 2$, $p < 0.05$). (c) Membrane resistance (R_M), fouling resistance (R_{HA}), and HA mass desorbed from the membrane surface after the fouling test. (d) NaCl rejection of the membranes having been exposed to 2000 mg/L NaOCl solution for 5 hours. The pH of the NaOCl solution was adjusted to 4, 7, or 10 with dilute HCl and NaOH.

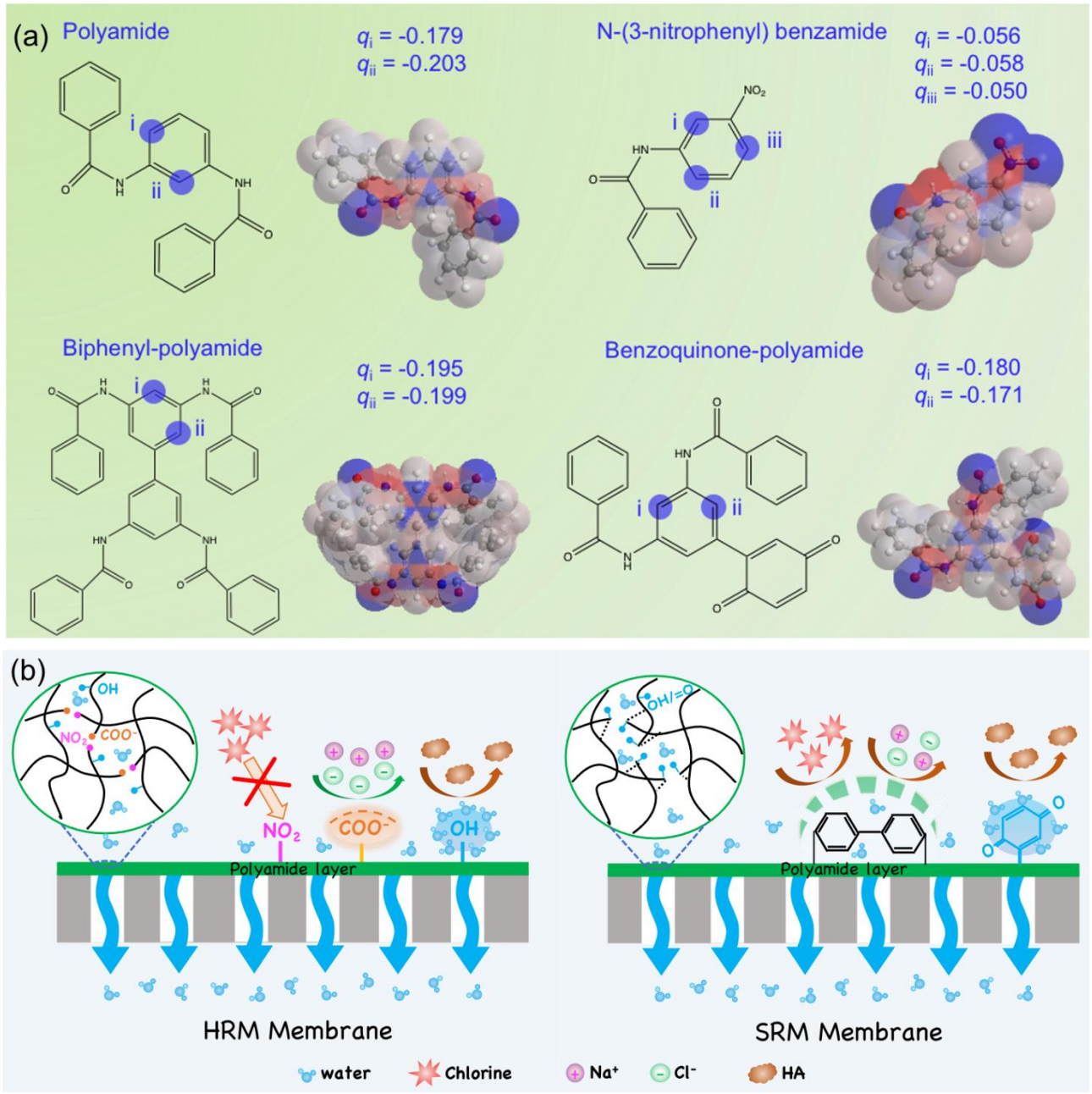

Figure 5. (a) Extended Huckel atomic charge analysis of the typical moieties (polyamide structure, N-(3-nitrophenyl) benzamide, biphenyl-polyamide structure, and benzoquinone-polyamide structure) in the pristine and modified polyamide membranes. The analysis was obtained from Chem3D program (19.1 version). (b) Schematic illustration of the performance enhancement in terms of water flux, fouling- and chlorine-resistance of the hydroxyl radical-modified (HRM) and sulfate radical-modified (SRM) membranes.